An electron diffraction and lattice dynamical study of thermal diffuse scattering in KCl

1989 J. Phys.: Condens. Matter 1 2305

(http://iopscience.iop.org/0953-8984/1/13/002)

J. Phys.: Condens. Matter 1 (1989) 2305–2311. Printed in the UK

An electron diffraction and lattice dynamical study of thermal diffuse scattering in KCl

G L Hua, T R Welberry and R L Withers
Research School of Chemistry, The Australian National University, GPO Box 4, Canberra, ACT 2601, Australia

Received 18 July 1988, in final form 25 November 1988

Abstract. Strong diffuse scattering characterised by blobs ('spots') of diffuse intensity well separated from neighbouring Bragg peaks and by diffuse streaks perpendicular to the $\langle 100 \rangle^*$ directions have been observed in zone axis electron diffraction patterns of KCl. An *ab initio* lattice dynamical investigation based on the shell model has been performed and the intensity of thermal diffuse scattering calculated from the dispersion relations obtained. The calculated results indicate that the rather strong and characteristic diffuse intensity distribution of KCl can, at least qualitatively, be well understood in terms of the thermal excitation of low-energy phonon modes.

1. Introduction

The beginnings of the work reported in this paper lie in the simple observation that characteristic and quite striking thermally induced diffuse intensity distributions are frequently observed (and equally frequently ignored!) in electron diffraction patterns of solids—an observation first pointed out by Honjo *et al* (1964) and Harada and Honjo (1965) almost 25 years ago. The study of lattice vibrations in solids is nowadays undoubtedly best carried out by means of inelastic neutron scattering, if large enough single crystals are available, and if the particular material involved does not have too large an absorption cross section for neutrons. Frequently, however, these latter conditions are not met. The study of lattice vibrations in solids is then best studied via the observation and/or quantitative measurement of thermal diffuse scattering (TDS). Such studies have a rather long and fascinating history (Preston 1936, 1938, Laval 1938, Boccara 1960). Most have been made by means of x-ray diffraction, because much smaller single crystals are needed than for neutron diffraction and because such measurements can be put on a quantitative basis and used, in favourable cases, to extract phonon dispersion relations (see, e.g., Buyers and Smith 1966).

By contrast, electron diffraction studies of diffuse intensity distributions have tended to remain qualitative owing to the difficulties of quantitative intensity measurement and of taking multiple scattering (or dynamical diffraction) into account. The great advantage of electron diffraction, however, is that it provides a much quicker initial survey of reciprocal space (and of any unusual features contained therein) than can be obtained with any other diffraction technique. In addition, such diffraction patterns can be taken from localised areas, thus obviating the need for large (0.1 mm or more) single crystals.

0953-8984/89/132305 + 07 $02.50

Table 1. The input data

Property	Input data	Units	Reference
m_1	39.10	au	
m_2	35.45	au	
r	3.117	10^{-10} m	Singh and Nirwal (1979)
C_{11}	0.4832	10^{11} Pa	Dochy (1980)
C_{12}	0.0540	10^{11} Pa	Dochy (1980)
C_{44}	0.0663	10^{11} Pa	Dochy (1980)
ε_0	4.49		Dochy (1980)
ε_∞	2.20		Dochy (1980)
β	2.09	10^{10} Pa	Basu and Sengupta (1980)
ω_{lo}	6.462	10^{12} s^{-1}	Raunio and Almqvist (1969)
ω_{to}	4.463	10^{12} s^{-1}	Raunio and Almqvist (1969)

This capacity made possible the recent discovery of a rather spectacular diffuse intensity distribution in β-cristobalite (Hua *et al* 1988). In the case of KCl, large single crystals are, of course, available and the phonon dispersion relations have already been accurately measured along the principal reciprocal lattice directions. Hence one is unlikely to learn any more about the lattice dynamics of KCl via an electron diffraction study. Nevertheless, it was still considered to be of interest to calculate the TDS of KCl, to compare it with the rather strong and characteristic diffuse intensity distribution observed in its room-temperature electron diffraction patterns—particularly those taken in the vicinity of the $[11\bar{2}]$ and $[11\bar{3}]$ zone axis orientations (figure 2, later)—and hence to demonstrate the sensitivity of electron diffraction to thermal vibration. The desire to understand, at least qualitatively, the streaks and 'spots' on such electron diffraction patterns provided the specific impetus for this study. The absence of any characteristic substructure in electron micrographs, plus the fact that diffuse streaking could be seen for almost any incident beam orientation, strongly suggested that the diffuse intensity distribution was due solely to the thermal excitation of low energy phonon modes.

Although KCl is known to suffer fairly severe radiation damage when observed at room temperature in electron microscopes under high-current-density conditions (Hobbs *et al* 1973, Hobbs 1979), the types of defect produced and their concentration (even under the worst possible scenario—and care was taken to minimise radiation damage as far as possible) are simply incapable of explaining the highly structured diffuse intensity distribution observed experimentally (Hughes and Pooley 1971, Catlow *et al* 1980, Hobbs *et al* 1973). An attempt was made to verify the thermal origin of the diffuse intensity distribution via heating experiments in an electron microscope hot stage. For temperatures greater than about 50 °C, however, it was found that the electron beam rapidly thinned the KCl crystals. Indeed, focusing of the beam caused well localised holes to be 'drilled' in every grain tested within the space of a few seconds! This is presumably equivalent to the 'electron beam flashing' technique originally reported by Honjo and Yagi (1963) and subsequently developed as a method for micro-writing using an electron beam (see, e.g., Humphreys *et al* 1985).

In order to calculate the intensity of TDS at any point in reciprocal space, it is of course necessary to have an appropriate force constant model. In the case of the alkali halides, such models are not hard to come by. Since the pioneering work on NaCl with the rigid-ion model by Kellermann (1940), a number of quite successful lattice dynamical models have been developed. Among these are the deformation dipole model (Hardy and Karo

1959, 1960) and the shell model (Dick and Overhauser 1958, Woods *et al* 1960) (these take the polarisability of the ions into consideration), the breathing-shell model (Schröder 1966, Nüsslein and Schröder 1967), the deformable shell model (Basu and Sengupta 1968) and the three-body force shell model (Verma and Singh 1969)—all of which further include the many-body interactions in different forms. Attempts to develop various microscopic models based on electronic wavefunctions have also been reported in the literature (Wakabayashi and Sinha 1974, Zeyher 1975, Basu and Sengupta 1980).

We should emphasise again here that the intention of this work is not to develop yet another lattice dynamical model which might be in better agreement with experimental phonon data. Rather it is simply to adapt suitably one of the existing models in order to calculate the intensity of thermal diffuse scattering and, hence, to allow a qualitative comparison with observed electron diffraction patterns to be made. It was not, therefore, considered necessary to use the most sophisticated model available. We have used the shell model in this investigation.

2. Force constant model

The general theory of the shell model is available with great detail in the literature (Cowley *et al* 1963). Therefore, we present here only briefly the model employed in our investigation. Under the well known adiabatic, harmonic and electrostatic approximations, the shell model takes into account the finite polarisability of the individual ions. The ions are polarised by the variation in the electric field stimulated by the lattice vibration. Each ion is considered as made up of a rigid core with a surrounding spherical shell of charge which is attached to the core by a spring. The short-range repulsive forces are assumed to be of the axially symmetric central type and involve core–core, shell–shell and core–shell interactions. The long-range Coulomb interaction is expressed as a dimensionless coefficient introduced by Kellermann (1940) and calculated by the Ewald (1921, 1938) method. The general formula of the equations of motion are given in the work of Cowley *et al* (1963).

In our calculation, both negative and positive ions were considered to be polarised. The model thus has 11 parameters. The short-range forces include not only the nearest-neighbour interactions A_{12} and B_{12} between the positive and negative ions but also the second-nearest-neighbour interactions A_{11}, B_{11}, A_{22} and B_{22} between the same type of ions. The total electronic charge on the ions is expressed as Z. The charges on the shells and the stiffness of the springs for the ions are specified separately as Y_1, Y_2 and K_1, K_2. The parameters Y and K can also be represented in terms of quantities which are more

Table 2. Shell model parameters from the least-squares fitting. The error $\Delta = \Sigma_i |f_i - f_{io}|/n$.

A_{12}	10.778	B_{12}	−0.839
A_{11}	−0.459	B_{11}	0.527
A_{22}	0.559	B_{22}	−0.204
Y_1	−4.560	K_1	5.544×10^3 N m^{-1}
Y_2	−0.282	K_2	1.834×10^3 N m^{-1}
α_1	0.864×10^{-30} m^3	d_1	0.028
α_2	0.010×10^{-30} m^3	d_2	0.005
ZZ	0.760	Δ	0.066×10^{12} s^{-1}

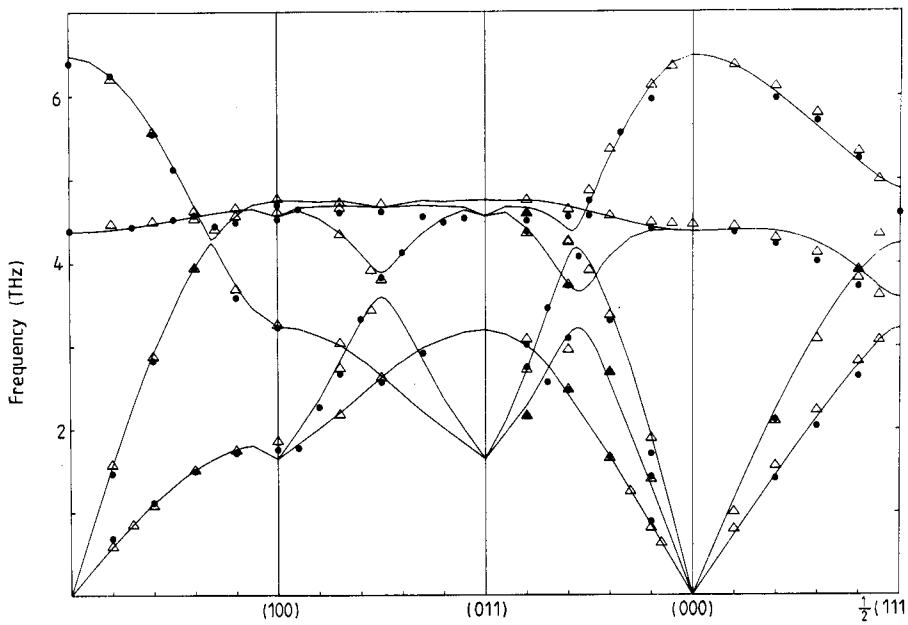

Figure 1. Phonon dispersion curves (——) for KCl calculated from the shell model parameters in table 1. The experimental phonon data from Raunio and Almqvist (1969) (△) and those from Copley *et al* (1969) (●) are also presented in the figure for comparison.

physically meaningful. These quantities are the electrical polarisabilities α of the ions and the short-range or mechanical polarisabilities d.

The force constant parameters were initially calculated with the input data from table 1. They were then applied to the equations of motion. The calculated phonon frequencies were fitted to the experimental data from Raunio and Almqvist (1969) along the three main symmetric directions. The fitting program is a standard FORTRAN program DUNLSF from the IMSL subroutine library, which uses a modified Levenberg–Marquardt algorithm and a finite-difference Jacobian to solve the non-linear least-squares problem. The force constant parameters obtained from the fitting process were then used to calculate dispersion curves along general reciprocal lattice directions and the corresponding first-order TDS. The final error between the calculated and the measured phonon frequencies is measured by the quantity $\Delta = \Sigma_i|f_i - f_{io}|/n$, where f_i are the calculated and f_{io} the observed frequencies. The force constant parameters obtained from the fitting process are listed in table 2. The dispersion curves of KCl along the three main symmetric directions and an off-symmetric direction are presented in figure 1. The experimental phonon data from Raunio and Almqvist (1969) and from Copley *et al* (1969) are also presented in the same figure for comparison.

The method of calculating the first-order TDS was described in detail in an earlier investigation in NiAs (Hua *et al* 1988) and will not be repeated here. We have calculated the relative intensity of the thermally induced diffuse intensity distribution for reciprocal lattice sections perpendicular to several different zone axes. Three of these are presented for comparison with the corresponding electron diffraction patterns of figure 2 in figure 3. For comparison with the observed electron diffraction photographs, the intensity was calculated over one quadrant of the zone required, on a grid of 40 × 40 points. Symmetry was used in order to generate the other three quadrants.

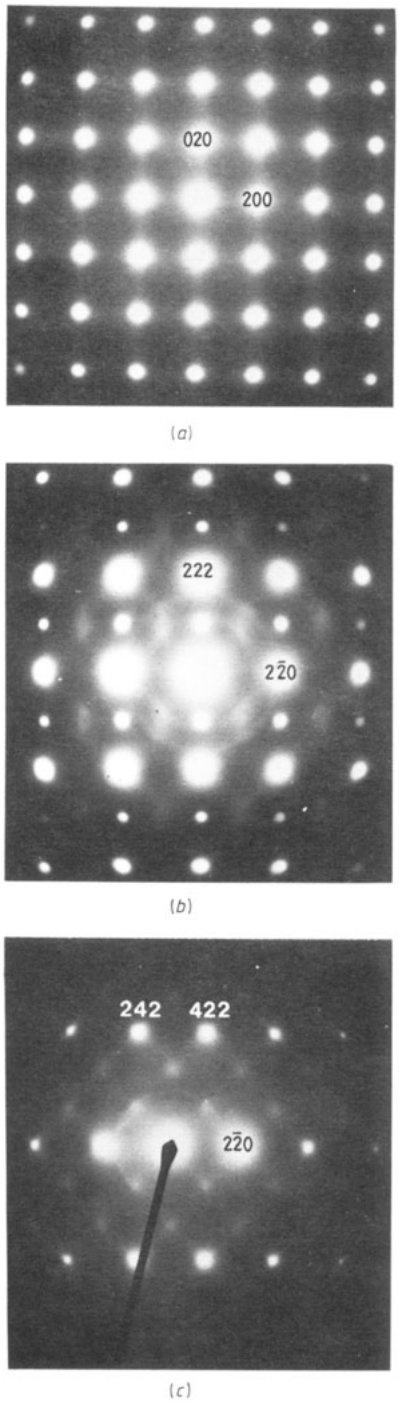

Figure 2. (*a*) ⟨100⟩, (*b*) ⟨11$\bar{2}$⟩ and (*c*) ⟨11$\bar{3}$⟩ zone axis electron diffraction patterns of KCl at room temperature. Note the diffuse streaks perpendicular to ⟨100⟩ directions in (*a*)–(*c*) and the characteristic blobs of diffuse intensity (well separated from neighbouring Bragg peaks) in (*b*) and (*c*).

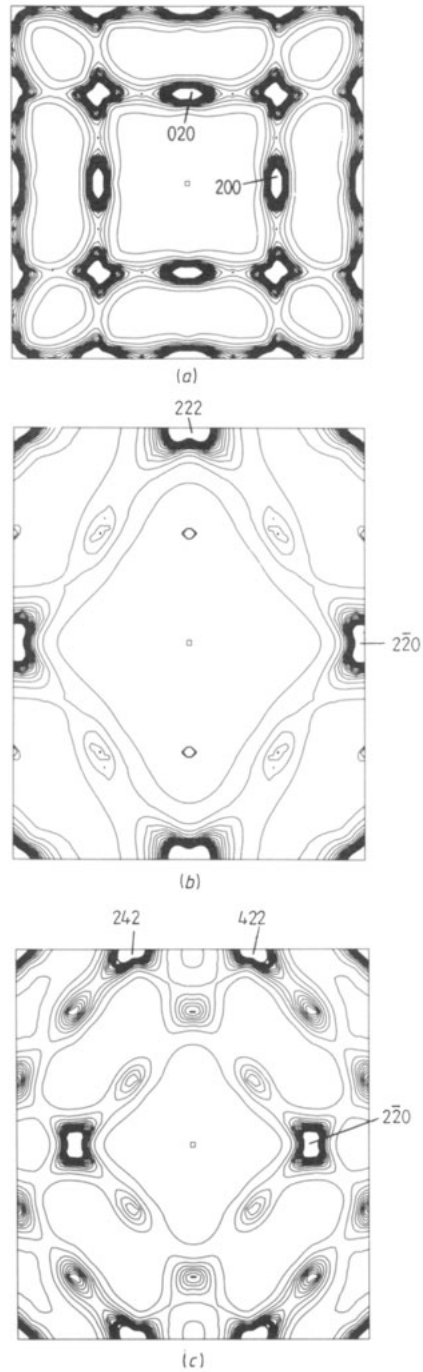

Figure 3. Contour plots of the calculated diffuse intensity distribution for reciprocal lattice sections perpendicular to (*a*) ⟨100⟩, (*b*) ⟨11$\bar{2}$⟩ and (*c*) ⟨11$\bar{3}$⟩ zone axis.

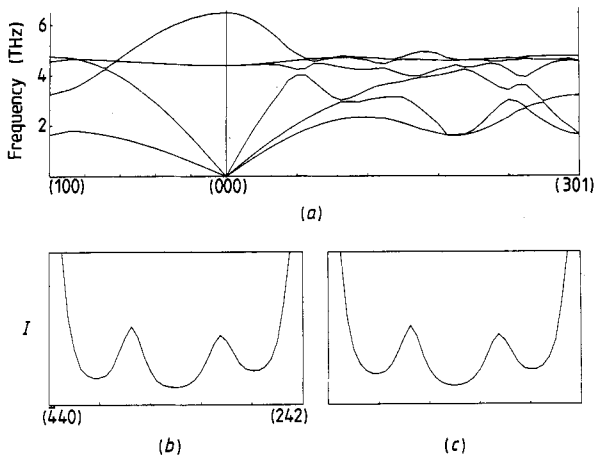

Figure 4. (*a*) Phonon dispersion curves along the (100)* and (301)* reciprocal lattice directions. The dip of the lowest transverse acoustic branches at the special wavevector $\frac{2}{3}(301)^*$ corresponds to the diffuse 'spots' in figure 2(*c*). (*b*) The combined contribution from the two lowest-energy phonon branches to the calculated diffuse intensity along the line $(\bar{4}40)^*$ to $(242)^*$. (*c*) The total contribution from all phonon branches to the calculated diffuse intensity along the line $(\bar{4}40)^*$ to $(242)^*$.

3. Results and discussion

The calculated diffuse intensity distributions shown in figure 3 are clearly in good qualitative agreement with the corresonding electron diffraction patterns in figure 2 and the thermal origin of the observed diffuse intensity distribution is thus established.

The most immediately striking feature of the observed diffuse patterns are the diffuse blobs or 'spots' at $\boldsymbol{G} \pm \frac{1}{3}(602)^*$ and $\boldsymbol{G} \pm \frac{1}{3}(062)^*$ in figure 2(*c*) and at $\boldsymbol{G} \pm (201)^*$ and $\boldsymbol{G} \pm (021)^*$ in figure 1(*b*) (where $\boldsymbol{G}$ is an allowed matrix reflection). In addition to these blobs, diffuse intensity localised in sheets perpendicular to the $\langle 100\rangle^*$ directions and running through the strong Bragg reflections is also visible (Honjo *et al* (1964) similarly reported the existence of such diffuse sheets of intensity, but perpendicular to both the $\langle 100\rangle^*$ and the $\langle 110\rangle^*$ reciprocal lattice directions; we find no evidence for the latter). The origin of the diffuse sheets perpendicular to the $\langle 100\rangle^*$ directions lies in the substantial excitation of low-frequency transverse acoustic phonon modes characterised by phonon wavevectors perpendicular to $\langle 100\rangle^*$ and with polarisation displacements parallel to $\langle 100\rangle$. Along $\langle 100\rangle^*$ reciprocal lattice directions (figure 4(*a*)), this lowest-frequency transverse acoustic phonon branch is doubly degenerate. On moving away from these high-symmetry directions, but remaining perpendicular to an $\langle 010\rangle^*$ direction (e.g. along $(301)^*$), this pair of doubly degenerate branches splits and both frequencies in general rise somewhat (see figure 4(*a*)). The lowest branch gives rise to diffuse intensity at $\boldsymbol{G} \pm \alpha(301)^*$ and, in general, to sheets of diffuse intensity perpendicular to $\langle 010\rangle^*$. The second-lowest branch, however, contributes little to the TDS until it is forced to become nearly degenerate with the lowest branch in the vicinity of certain special points. For example, along the $(301)^*$ reciprocal lattice direction, one such special point occurs at $\frac{2}{3}(301)^* = (20\frac{2}{3})^*$. Because $\omega_j(\boldsymbol{q}) \equiv \omega_j(\boldsymbol{G} + \boldsymbol{q})$ (where $\boldsymbol{G}$ is an allowed matrix reflection), $\omega_j(20\frac{2}{3})^* \equiv \omega_j(00\frac{2}{3})^*$. At such phonon wavevectors, this lowest branch is constrained by symmetry to be doubly degenerate (see figure 4(*a*)). In the vicinity of such special points, the contribution of the second-lowest branch to the TDS rises sharply and it is this effect which gives rise to the apparent extra 'spots' in figures 1(*b*) and 1(*c*). Figure 4(*b*), for example, shows the combined contribution of branches 1 and 2 to the TDS along the line $(\bar{4}40)^*$ to $(242)^*$ of figure 2(*c*). Figure 4(*c*) shows the total contribution from all the branches to the TDS along the same line. An alternative way of understanding the existence of the blobs along such $(h0l)^*$ directions in reciprocal space can be obtained

from figure 2(*a*). Consider, for example, an imaginary line drawn between the origin and (620)* in figure 2(*a*). In progressing from the origin to (620)*, the diffuse sheets of intensity are crossed twice—hence the two diffuse blobs in figure 2(*c*) in this region of reciprocal space. In conclusion, it is clear that the rather strong and characteristic diffuse intensity distribution of KCl can, at least qualitatively, be well understood in terms of the thermal excitation of low-energy phonon modes.

References

Basu A N and Sengupta S 1968 *Phys. Status Solidi* **29** 367
—— 1980 *Phys. Status Solildi* **102** 117
Boccara N 1960 *C.R. Acad. Sci., Paris* **250** 1025
Buyers W J L and Smith T 1966 *Phys. Rev.* **150** 758
Catlow C R A, Diller K M and Hobbs L W 1980 *Phil. Mag.* A **42** 123–50
Copley J R D, Macpherson R W and Timusk T 1969 *Phys. Rev.* **182** 965
Cowley R A, Cochran W, Brockhouse B N and Woods A D B 1963 *Phys. Rev.* **131** 1030
Dick B G and Overhauser A W 1958 *Phys. Rev.* **112** 90
Dochy F 1980 *Phys. Status Solidi* **59** 531
Ewald P P 1921 *Ann. Phys., Lpz.* **64** 253
—— 1938 *Nachr. Ges. Wiss. Göttingen, N.F.II* **3** 55
Harada J and Honjo G 1965 *Int. Conf. Electron Diffraction and Crystal Defects, (Melbourne) 1965*
Hardy J R and Karo A M 1959 *Phil. Mag.* **4** 1278
—— 1960 *Phil. Mag.* **5** 859
Hobbs L W 1979 *Introduction to Analytical Electron Microscopy* ed. J J Hren, J I Goldstein and D C Joy (New York: Plenum) pp 437–80
Hobbs L W, Hughes A E and Pooley D 1973 *Proc. R. Soc.* A **332** 167–85
Honjo G, Kodera S and Kitamura N 1964 *J. Phys. Soc. Japan* **19** 351
Honjo G and Yagi K 1963 *J. Phys. Soc. Japan. Suppl.* II **18** 355
Hua G L, Welberry T R and Withers R L 1988 *J. Phys. C: Solid State Phys.* **21** 3863–76
Hua G L, Welberry T R, Withers R L and Thompson J G 1988 *J. Appl. Crystallogr.* **21** 458–65
Hughes A E and Pooley D 1971 *J. Phys. C: Solid State Phys.* **4** 1963–76
Humphreys C J, Salisbury I G, Berger S D, Timsit R S and Mochel M E 1985 *Electron Microscopy and Analysis 1985* (Inst. Phys. Conf. Ser. 78) pp 1–6
Kellermann E W 1940 *Phil. Trans. R. Soc.* A **238** 513
Laval J 1938 *C.R. Acad. Sci., Paris* **207** 169
Nüsslein V and Schröder U 1967 *Phys. Status Solidi* **21** 309
Preston G D 1936 *Proc. R. Soc.* A **167** 526
—— 1938 *Proc. R. Soc.* A **172** 116
Raunio G and Almqvist L 1969 *Phys. Status Solidi* **33** 209
Schröder U 1966 *Solid State Commun.* **4** 347
Singh R K and Nirwal V V S 1979 *Nuovo Cimento* **52b** 113
Verma M P and Singh R K 1969 *Phys. Status Solidi* **33** 769
Wakabayashi N and Sinha S K 1974 *Phys. Rev.* B **10** 745
Woods A D B, Cochran W and Brockhouse B N 1960 *Phys. Rev.* **119** 980
Zeyher R 1975 *Phys. Rev. Lett.* **35** 174